

OPEN ACCESS

Ionic Liquid Electrolytes for Metal-Air Batteries: Interactions between O₂, Zn²⁺ and H₂O Impurities

To cite this article: D. Alwast *et al* 2020 *J. Electrochem. Soc.* **167** 070505

View the [article online](#) for updates and enhancements.



Ionic Liquid Electrolytes for Metal-Air Batteries: Interactions between O₂, Zn²⁺ and H₂O Impurities

D. Alwast,^{1,2} J. Schnaidt,^{1,2} Z. Jusys,^{1,*} and R. J. Behm^{1,2,z}

¹Institute of Surface Chemistry and Catalysis, Ulm University, Ulm, Germany

²Helmholtz-Institute Ulm (HIU) Electrochemical Energy Storage, Ulm, Germany

³Karlsruhe Institute of Technology (KIT), Karlsruhe, Germany

Motivated by the potential of ionic liquids (ILs) to replace traditional aqueous electrolytes in Zn-air batteries, we investigated the effects arising from mutual interactions between O₂ and Zn(TFSI)₂ as well as the influence of H₂O impurities in the oxygen reduction/oxygen evolution reaction (ORR/OER) and in Zn deposition/dissolution on a glassy carbon (GC) electrode in the ionic liquid N-butyl-N-methylpyrrolidinium bis(trifluoromethanesulfonyl)-imide (BMP-TFSI) by differential electrochemical mass spectrometry. This allowed us to determine the number of electrons transferred per reduced/evolved O₂ molecule. In O₂ saturated neat BMP-TFSI the ORR and OER were found to be reversible, in Zn²⁺ containing IL Zn deposition/stripping proceeds reversibly as well. Simultaneous addition of O₂ and Zn²⁺ suppresses Zn metal deposition, instead ZnO₂ is formed in the ORR, which is reversible only after excursions to very negative potentials (−1.4 V). The addition of water leads to an enhancement of all processes described above, which is at least partly explained by a higher mobility of O₂ and Zn²⁺ in the water containing electrolytes. Consequences for the operation of Zn-air batteries in these electrolytes are discussed.

© The Author(s) 2019. Published by ECS. This is an open access article distributed under the terms of the Creative Commons Attribution Non-Commercial No Derivatives 4.0 License (CC BY-NC-ND, <http://creativecommons.org/licenses/by-nc-nd/4.0/>), which permits non-commercial reuse, distribution, and reproduction in any medium, provided the original work is not changed in any way and is properly cited. For permission for commercial reuse, please email: oa@electrochem.org. [DOI: 10.1149/2.0052007JES]



Manuscript submitted September 11, 2019; revised manuscript received November 1, 2019. Published December 4, 2019. *This paper is part of the JES Focus Issue on Challenges in Novel Electrolytes, Organic Materials, and Innovative Chemistries for Batteries in Honor of Michel Armand.*

The major advantage of primary Zn-air batteries is their high energy density, which is about five times higher than the one of Li-ion batteries.^{1–3} Therefore, primary Zn-air batteries are already commercially used in applications where their low power output capability (<10 mW) caused by the inefficiency of the air catalysts, is no significant drawback, e.g., in hearing aids.² This is different, however, for secondary Zn air batteries, which suffer from several drawbacks such as dendrite growth, limited solubility of the discharge product and insufficient performances of the bifunctional air electrodes.^{4,5} These problems have so far precluded their technical realization. Therefore, the reversibility of the oxygen reduction reaction (ORR) and of the oxygen evolution reaction (OER) during discharge and charge of the battery is a key issue for improving Zn-air batteries.^{2,6–10} The cathode side of Zn-air batteries usually consists of a porous carbon electrode covered by a catalyst layer to facilitate the ORR.^{3,7} The porous electrode enables O₂ diffusion to the three-phase boundary region.³ This, however, also allows CO₂ diffusion into and H₂O evaporation out of the cell, which are additional drawbacks since the CO₂ in the cell will react with the OH[−] ions of the alkaline electrolyte and form carbonates, which reduces the lifetime of the cell.¹¹ Additionally, H₂O evaporation leads to drying-out of the cell.^{12,13} Considering these drawbacks, ILs seem to be promising candidates for electrolytes in secondary metal-air batteries, as most of them show a very low volatility and a wide electrochemical stability window as compared to aqueous electrolytes.^{7,14–16} The lower volatility could solve the problem of cell dry-out. Due to the wide electrochemical window H₂ evolution could be avoided, and furthermore there are ILs available which are insensitive against water and CO₂. Finally, the absence of OH[−] ions precludes carbonate formation. However, the low conductivity and high viscosity are still drawbacks for the use of ILs in (metal-air) batteries. On the other hand, due to the open cell design of metal-air batteries, moisture from the air can diffuse into the cell and change the electrochemical behavior of the electrolyte, which in the case of ionic liquids can result in a reduced viscosity and higher conductivity of the electrolyte.¹⁷ Accordingly, the influence of water on the electrochemical properties of Zn-air batteries and on the performance of the ORR/OER and the Zn

plating/stripping processes, as the main processes in these batteries, in IL electrolyte is of considerable interest. These aspects are topic of the present paper, focusing on N-butyl-N-methylpyrrolidinium bis(trifluoromethanesulfonyl)imide (BMP-TFSI) based electrolytes.

There are already a number of studies on the influence of water on the Zn deposition and dissolution behavior in various ILs, focusing mostly on the effect of water on the morphology of the resulting deposits, but also dealing with the reaction rate and the reversibility of the Zn redox couple.^{15,17–20} More specifically, for BMP-TFSI Xu et al. concluded that on Pt electrodes the redox reversibility of the Zn/Zn(II) redox couple is improved and the reaction rate is increased upon addition of water.¹⁷ At (too) high water levels this leads to a decrease of the electrochemical stability window.¹⁷

Furthermore, it is well known that water has an impact also on the ORR and OER in ionic liquids. For the ORR this generally results in an earlier onset of the reaction and higher currents in the presence of water.^{21–24} For the OER the results reported so far are less clear. AlNashef et al. did not find an oxidation peak in the anodic scan after the ORR in the O₂-containing ILs 1-n-butyl-3-methylimidazolium hexafluorophosphate and 1,2-dimethyl-3-n-butylimidazolium hexafluorophosphate on a glassy carbon (GC) electrode after the addition of 3 wt% water. This they explained by a (chemical) disproportionation of the superoxide, forming O₂ (2 O₂^{•−} + H₂O → O₂ + HOO[−] + HO[−]).²¹ In contrast to this, Katayama et al. observed an anodic peak in cyclic voltammograms (CVs) in O₂-saturated, humidified (0.5 vol% of water) EMIM-TFSI after the reduction reaction and attributed this to the re-oxidation of either HO₂ or H₂O₂.²² This anodic peak occurred at higher potentials compared to dry conditions, indicating that the addition of water hinders the OER.²² Xiong et al. also found the OER to be hampered, but not fully inhibited in humid atmosphere (relative humidity 8%, 25% and 36%) in phosphonium cation based ILs.²³ Furthermore, also the presence of metal cations is known to influence the ORR/OER in ILs and aprotic organic electrolytes.^{25–28} For instance, it has been demonstrated by XRD measurements that in the presence of Zn²⁺ the ORR results in the deposition of ZnO films, which are likely to hinder the ongoing ORR/OER.^{29–31}

Here we report results of a study on Zn deposition/dissolution on glassy carbon (GC) electrodes in dry and humidified BMP-TFSI, where we tried to disentangle Zn deposition and electrolyte decomposition, by using a differential electrochemical mass spectrometry

*Electrochemical Society Member.

^zE-mail: juergen.behm@uni-ulm.de

(DEMS) setup, which would allow us to detect, e.g., H_2 evolution caused by the degradation of the electrolyte. These results, which are presented in the first results section, can serve also as reference for the subsequent ORR/OER measurements in the presence of Zn^{2+} . Furthermore, we used DEMS measurements to identify and quantify the consumption/evolution of O_2 in the ORR and OER, respectively, in parallel with the electrochemical measurement. This allows us to determine the numbers of transferred electrons during the ORR from the ratio between the reduction current and the O_2 consumption, which allows the identification of the main species formed in the reactions, i.e., superoxide (O_2^-), peroxide (O_2^{2-}) or oxide (O^{2-}), if no other reactions take place in parallel (i.e. H_2 evolution; metal deposition), providing insight into the reaction mechanisms. Furthermore, the detection of O_2 during the anodic scan provides direct proof that anodic peaks are related to the OER and do not result from side reactions such as electrolyte decomposition or electrode modification. These results are presented and discussed in the second results section. Third, we studied the effect of Zn^{2+} addition on the ORR/OER by DEMS, which provides additional information on the number of transferred electrons during the cathodic scan, and on the reversibility with respect to O_2 evolution in the anodic scan. These results are presented and discussed in the third result section. Next, in the fourth section we present results on the combined effect of water impurities and Zn^{2+} on the ORR/OER in an O_2 saturated ternary electrolyte mixture containing BMP-TFSI, ZnTFSI_2 and H_2O . Finally the results are summarized and discussed in a comprehensive picture.

Experimental

For the experiments, we used a DEMS setup (potentiostat: Pine Instruments, AFRDE 5; quadrupole mass spectrometer: Pfeiffer Vacuum, QMS 422) which has been described in detail recently.²⁵ Its core part is a dual thin-layer flow cell with a non-porous 10 μm thick Teflon membrane, separating the electrolyte from the mass spectrometer chamber.

BMP-TFSI (99.9%, halides ≤ 1 ppm; $\text{H}_2\text{O} \leq 20$ ppm) and $\text{Zn}(\text{TFSI})_2$ (99.5%, H_2O content ≤ 100 ppm) were purchased from Solvionic. The electrolytes (neat BMP-TFSI and 0.01 M $\text{Zn}(\text{TFSI})_2$ in BMP-TFSI) were transferred through air into a vacuum chamber, which was used for drying and storing the electrolytes. Here the ILs were evacuated prior to use at 10^{-7} mbar for >12 h for drying, which resulted in a water content of 60 ppm in BMP-TFSI, and also saturated with O_2 (MTI, N 6.0).³² For the measurements the electrolyte was pumped in a loop between the vacuum chamber and the flow cell by a peristaltic pump (Ismatek, Reglo ICC) with a flow rate of 0.16 mL min^{-1} (total volume 10 mL).^{25,32} The capillary system was surrounded by N_2 -flushed tubes to reduce the amount of moisture and O_2 diffusing through the capillary walls. For the measurements with humidified electrolyte, O_2 was first saturated with water by bubbling it through a water-filled washing bottle at 23°C and then bubbled into the electrolyte reservoir in the vacuum chamber. The water content of the humidified electrolyte was determined by Karl-Fischer titration to $0.8 \pm 0.03 \text{ wt\%}$ (0.62 mol l^{-1} ; 15.9 at%) in neat BMP-TFSI and $1.1 \pm 0.03 \text{ wt\%}$ (0.85 mol l^{-1} ; 20.6 at%) in 0.01 M $\text{Zn}(\text{TFSI})_2$ in BMP-TFSI. In the following the term “dry” is used for the non-humidified electrolyte used after drying for >12 h in the vacuum chamber, which still contains traces of residual water.

As working electrode and counter electrode we used a glassy carbon (GC) disk (polished with a 0.3 μm alumina slurry prior to use) and a Pt wire (Goodfellow, 99.99+, diameter 0.5 mm), respectively. A Mg wire (Goodfellow, 99.99+, diameter 0.25 mm) with a native oxide film (Mg/MgO ; -1.0 vs. Fc/Fc^+) served as a quasi-reference electrode.³³ The sensitivity factor k^* of 3.4×10^{-7} of the DEMS measurements was determined assuming a one electron transfer ($n = 1$) for the first reduction step ($E > -0.4 \text{ V}$) of the ORR in neat BMP-TFSI, using the ratio between the ion current of the m/z 32 signal (i_{32}) and the faradaic current (i_F) according to the equation $k^* = nI_{\text{MS}}/i_F$.²⁵ Note that the ion currents plotted in following figures are corrected for

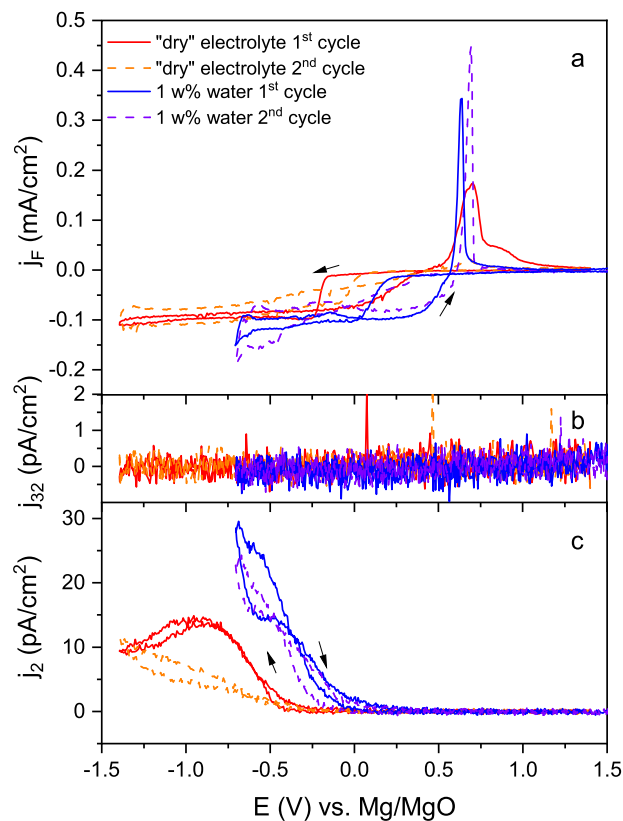


Figure 1. (a) CVs of N_2 purged “dry” (red, orange) and humidified (blue, purple) $\text{Zn}(\text{TFSI})_2$ containing BMP-TFSI (10 mV s^{-1} , 0.16 mL min^{-1}) on a GC electrode and the corresponding ion currents of (b) O_2 ($m/z = 32$) and (c) H_2 ($m/z = 2$).

the time delay due to mass transport of the gaseous species from the working electrode to and through the membrane.

The XRD patterns after electrochemical cycling were measured using a Siemens D5005 X-ray diffractometer with $\text{Cu-K}\alpha$ radiation ($\lambda = 1.542 \text{ \AA}$) in a 2θ range from 10 – 70° .

Results

Influence of H_2O on Zn deposition.—First, we investigated the influence of H_2O on the Zn deposition by DEMS. Figure 1a shows the first two CVs recorded in 0.01 M $\text{Zn}(\text{TFSI})_2$ containing BMP-TFSI in dried and humidified electrolyte, using a GC electrode. The CV in “dry” electrolyte exhibits the typical features for Zn deposition and dissolution in ionic liquid electrolytes, which are characterized by a cathodic peak due to the reduction of Zn^{2+} to Zn^0 and an oxidation peak in the anodic scan, together with a lower potential for the initial Zn^{2+} deposition.^{19,31,34,35} This leads to an overcrossing of the current in the anodic scan with that in the cathodic one at the potential where Zn^{2+} deposition changes to Zn dissolution. Such behavior, in particular the pronounced initial potential shift, was observed before during electrochemical deposition and it was attributed to initial nucleation processes.^{19,31,34,35} Our CVs differ, however, from those in previous reports by the absence of a distinct cathodic peak (Zn deposition) before approaching the mass transport limited current. The absence of this peak can easily be explained by the enforced mass transport in our case.

In the second (and following) cycle(s) the reduction in the cathodic scan starts at higher potentials than in the first one. The more facile Zn deposition may be induced by residual Zn nuclei on the surface, which promote Zn nucleation/growth in the following cycles and decrease the activation energy for further Zn nucleation.³⁵

The addition of water mainly causes a shift in the onset potential by 0.3 V to more positive values in the cathodic scan. This is accompanied by a sharper Zn dissolution peak in the anodic scan, whose onset occurs at slightly more negative potentials. The shift to higher potentials for Zn deposition might be attributed to changes in the nucleation behavior during Zn deposition. These and in particular the sharper Zn dissolution peak are likely related to changes in the physicochemical properties of the electrolyte, with the addition of water leading to a decreased viscosity and increased mobility of the Zn^{2+} species. Similar observations and interpretations were reported for the effect of water on the Zn redox behavior in different ILs,^{18,36} including also BMP-TFSI.¹⁷ The higher Zn^{2+} mobility additionally leads to a measurable increase of the mass transport limited current in the cathodic scan, resulting in a higher amount of deposited Zn during the scan.

Alternatively, the higher currents may also be attributed to H_2 evolution. The DEMS measurements resolve a clear increase at $m/z = 2$ (Figure 1c), indicative of H_2 evolution. This is assigned to the electrochemical degradation of residual water traces in the electrolyte ($2 \text{H}_2\text{O} + 2\text{e}^- \rightarrow 2 \text{OH}^- + \text{H}_2$). Both, in “dry” and in humidified electrolyte, the H_2 signal still increases when the faradaic current has already reached the mass transport limited region. Thus, the H_2 evolution reaction (HER) appears to be only a minor contribution to the overall faradaic current. As expected, the onset of the HER is at more positive potentials in the humidified electrolyte and higher HER rates are achieved.

Possible H_2 evolution from Zn corrosion in the presence of deposited Zn ($\text{Zn} + 2\text{H}_2\text{O} \rightarrow \text{Zn}(\text{OH})_2 + \text{H}_2$)^{1,3,37–39} cannot be fully excluded, but can only occur at negligible rates considering the absence of measurable $m/z = 2$ ion currents in the anodic scan at potentials where the Zn deposition is still in the mass transport limited region.

Finally we would like to note that the O_2 ion current ($m/z = 32$, Figure 1b) remains constant during cycling, indicating that there is no measurable reduction of residual O_2 in the electrolyte.

Influence of H_2O on ORR and OER.—The influence of H_2O on the electrochemical stability of BMP-TFSI is widely discussed and it is known, that an increasing H_2O content leads to a smaller electrochemical window (EW).^{17,40–42} Additionally, the presence of water was reported to have a promoting influence also on the ORR in ILs.^{21,24,40,43,44} In order to model the H_2O content of a system open to air, we introduced water to the system by purging the electrolyte with O_2 which was saturated with H_2O at 23°C.

In Figure 2 we compare the CVs and the ion currents of O_2 ($m/z = 32$) and H_2 ($m/z = 2$) during the ORR/OER in BMP-TFSI on a GC electrode in the presence (purple) and absence (black) of added water. Note that in contrast to the measurements in Zn^{2+} containing electrolyte shown in the first section we found no significant difference between the first and following cycles, indicating that the electrode surface is not modified by deposition of reaction products in the Zn^{2+} free electrolyte. Therefore, only the first cycle is depicted in Figure 2.

It has been reported previously that in dry, pure BMP-TFSI the first reduction step in the ORR on GC electrodes^{45,46} and Au electrodes²² is a one-electron transfer, forming a superoxide ion ($\text{O}_2 + \text{e}^- \rightleftharpoons \text{O}_2^{\cdot-}$), which is followed by a second one-electron reduction step, forming a peroxide ion ($\text{O}_2^{\cdot-} + \text{e}^- \rightarrow \text{O}_2^{2-}$) on GC^{25,47} and Au.²²

The faradaic currents of the “dry” BMP-TFSI measurements show both one-electron and two-electron reduction of O_2 , depending on the potential, similar to previous measurements with the same system performed in our group at a slower scan rate.²⁵ This allows us to calculate the intrinsic k^* value ($k^* = nI_{\text{MS}}/I_{\text{F}}$) of the DEMS-setup. Using the reduction in the current plateau at around 0 V as reference for a one-electron transfer, the second current regime (around -0.5 V) corresponds to a two-electron transfer. This points to predominant peroxide formation at low potentials. Interestingly, the potential difference between the two reduction ranges was reported to be around 1 V for a Au electrode,²² while for reduction on the GC electrode the potential difference between the plateaus (black curve, “dry” IL) is only 0.5 V. This may be related to the different electrode materials.

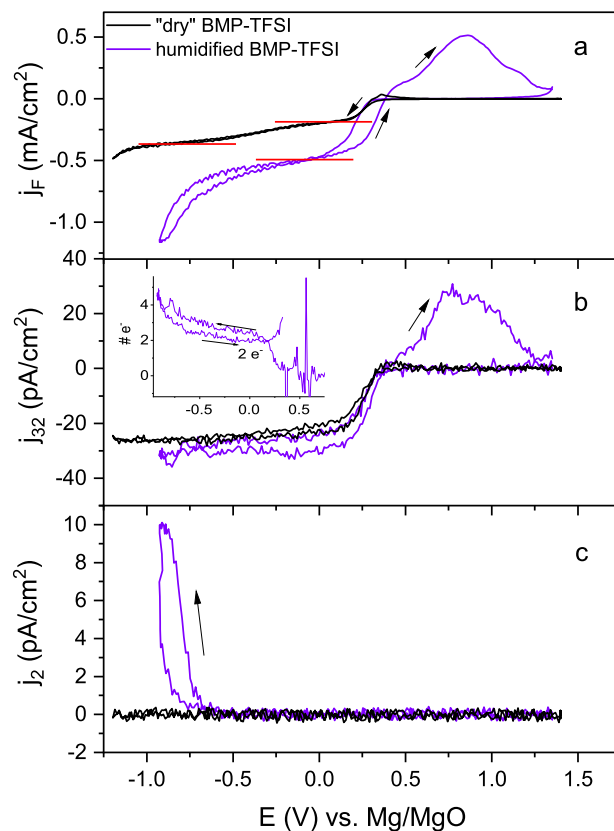


Figure 2. (a) CVs of ORR/OER in “dry” and H_2O containing BMP-TFSI and the corresponding ion currents of (b) O_2 ($m/z = 32$) and (c) H_2 ($m/z = 2$) (10 mV s^{-1} ; 0.16 mL min^{-1}). Inset: number of transferred electrons in humidified electrolyte.

We cannot rule out, however, that this discrepancy is influenced by water traces in our “dry” electrolyte. For instance, rotating ring disk electrode (RRDE) measurements by Yuan et al. showed that the addition of 0.25 wt% water leads to a shift of the two-electron reduction to more positive potentials by at least 0.2 V.⁴⁸ Moving to the humidified electrolyte, the two-electron transfer should be even more promoted, shifting its onset to more anodic potentials. Experimentally (see purple graphs in Figure 2), we observe the onset of the ORR in the humidified electrolyte at about the same potential as in “dry” electrolyte. However, only a single reduction range is visible, where about two electrons (2.3 e^- , see inset) are transferred per O_2 molecule during the reduction. Due to the presence of only a single reduction range, there is no internal reference with a single-electron transfer for determining the number of transferred electrons like in the “dry” electrolyte measurement. Therefore, we used the k^* value of the measurement in “dry” electrolyte for the evaluation (which may be slightly off due to different transport properties of O_2 in the humidified electrolyte). This results in values of the transferred electrons of about 2.3, which are rounded to 2 for further discussions. A two-electron transfer was calculated also by Yuan et al. from RRDE measurements on a Pt electrode in humidified BMP-TFSI.⁴⁹ From that number the authors concluded that after the addition of a significant amount of water (about 1 wt%) peroxide is formed upon reduction ($\text{O}_2 + \text{H}_2\text{O} + \text{e}^- \rightleftharpoons \text{HO}_2^{\cdot} + \text{OH}^-$; $2\text{HO}_2^{\cdot} \rightarrow \text{O}_2 + \text{H}_2\text{O}_2$).⁴⁸ Switzer et al. arrived at similar conclusions for the ORR in imidazolium-based trifluoromethanesulfonate electrolyte on Pt and GC electrodes, that the presence of an H^+ donor shifts the reaction to a two-electron or even four-electron process, depending on the electrode material.⁴³ They observed that after the addition of different protic additives, e.g., triflic acid or acetophenone, the ORR proceeds along a two-electron pathway on the GC electrode, and along a four-electron pathway on the Pt electrode. The ef-

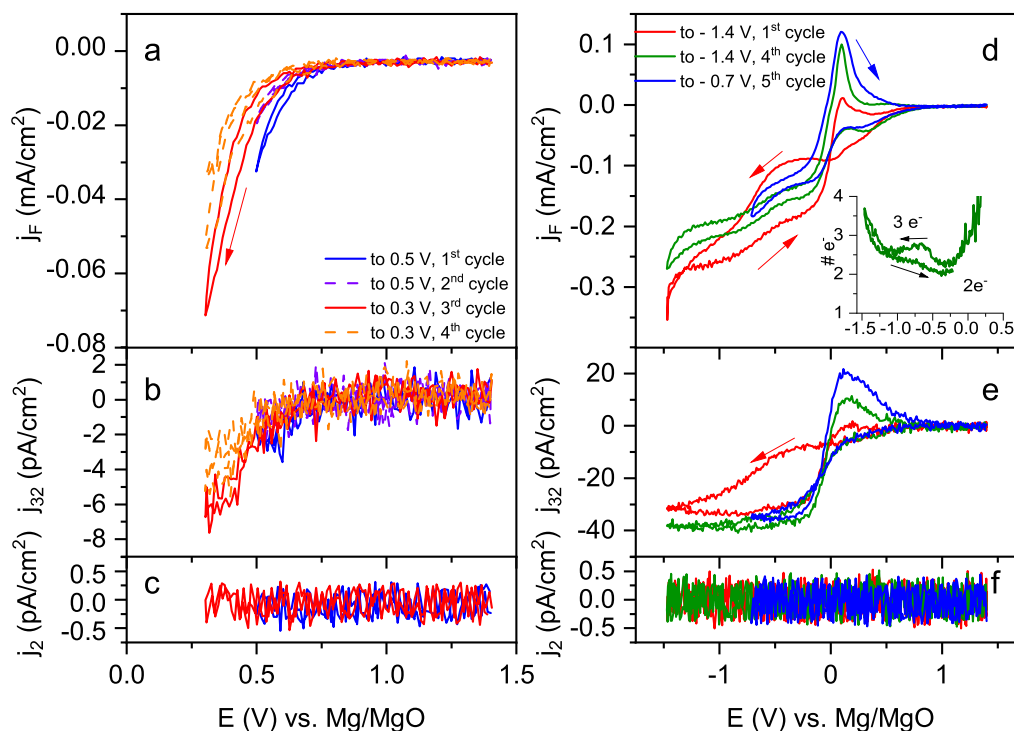


Figure 3. CVs of O_2 saturated 0.01 M $\text{Zn}(\text{TFSI})_2$ in BMP-TFSI (10 mV s^{-1} , 0.16 mL min^{-1}) on a GC electrode (top) and the corresponding ion currents of O_2 ($m/z = 32$) and H_2 ($m/z = 2$) with increasing (left) and decreasing (right) potential window. Inset: number of transferred electrons during the 4th cycle.

fect of the proton donors increases with increasing acidity/decreasing pK_a .⁴³ Nonetheless, we cannot completely exclude a contribution (<15%) from a four-electron pathway process on our GC electrode. Additionally, the faradaic current in the mass transport limited region of our measurement was found to increase upon the addition of water, without changing any other parameter. This increase, which is in line with the observations by Yuan et al. and Katayama et al. in water containing BMP-TFSI, can be explained by a lower viscosity, resulting in a higher mobility of O_2 upon the addition of a protic solvent.^{22,40,44} Also, the electrochemical window of the electrolyte is narrowed upon the addition of water to the electrolyte, as indicated by the increase of the cathodic current at potentials below $\sim -0.6 \text{ V}$. This increase is due to the evolution of H_2 , as shown by the corresponding signal in the ion current for $m/z = 2$. Thus, this current is due to water splitting rather than due to the decomposition of the IL. Nevertheless, we cannot rule out that part of the resulting current could also be due to the decomposition of BMP-TFSI, since it has been shown that water decreases its stability window.^{17,40–42} Furthermore, H_2 ($m/z = 2$) has been found as fragment of BMP-TFSI decomposition.⁵⁰

In the anodic scan in “dry” BMP-TFSI, a small peak appears in the faradaic current and also in the O_2 signal. This peak is attributed to the OER, oxidizing dissolved O_2^- .^{25,47} Although, the signals in the faradaic current (0.5% of the ORR current) and the ion current for $m/z = 32$ are small, the charge ratio between the two confirms a one-electron transfer during the OER. The main reason for the small signals is that the soluble superoxide and peroxide products formed in the cathodic scan are flushed away in the flowing electrolyte.

In humidified electrolyte the OER peak is much more pronounced. This result differs from part of the previous reports on the absence/appearance of an OER peak in humidified IL:^{14,21,22,40,44,51,52} AlNashef et al. did not find an OER peak after the addition of 3 wt% water in an imidazolium based ILs with a hexafluorophosphate anion on a glassy carbon electrode, which they explained by a water-induced destabilization of the superoxide, resulting in an irreversible formation of peroxide ($2 \text{O}_2^- + \text{H}_2\text{O} \rightarrow \text{O}_2 + \text{HOO}^- + \text{HO}^-$).²¹ This is in line with the interpretation and a CV reported in two papers by Yuan et al. for 1% water containing BMP-TFSI in O_2 atmosphere.^{40,44}

Unfortunately, in the second paper, these authors show another CV for the same electrolyte, but with a more negative (not specified) lower potential limit, which features two peaks in the anodic scan, where one of them appears at the expected OER potential.⁴⁰ Despite these inconsistencies, there is at least a rather constant anodic faradaic current in the anodic scan, which might be attributed to the OER (also from peroxide species). In contrast to the results by Yuan et al., increased peaks for the OER in humidified (compared to “dry”) ILs were reported by Katayama et al. (imidazolium based TFSI IL and a Au electrode)²² and Islam et al. (imidazolium based BF_4 IL and a Hg electrode),²⁴ which is in line with our results for humidified BMP-TFSI on a GC electrode (see Figure 2a).

A very similar peak we found also for the $m/z 32$ ion current (Figure 2b), which proves that it originates from the OER. The amount of O_2 evolved as measured by DEMS (integration between 0.3 and 1.4 V) points to the transfer of in average 1.5 electrons per O_2 molecule, which is explained by the oxidation of a mixture of superoxide and peroxide. This implies that not only superoxide, but also the peroxide formed during the ORR can be re-oxidized in BMP-TFSI.

The much more pronounced OER peak in humidified IL found in our flow cell experiments is surprising because dissolved intermediates (either superoxide or peroxide) should largely be flushed away as observed in the “dry” electrolyte. Thus, we conclude that the peroxide species formed in H_2O containing electrolyte largely remain at the working electrode and can there be oxidized again.

ORR and OER in Zn^{2+} containing BMP-TFSI.—As shown in the previous sections, the ORR in BMP-TFSI on GC takes place in the same potential window as Zn deposition (which for a Zn-air cell would result in a very low or no usable cell voltage). Thus, both processes could contribute to the cathodic faradaic current when the electrolyte contains both Zn^{2+} and O_2 . Furthermore, also the influence of the Zn^{2+} ions on the ORR product formation (and their possible deposition on the electrode surface) and on the OER are key issues for Zn-air batteries. In Figure 3 we present CVs of 0.01 M $\text{Zn}(\text{TFSI})_2$ in O_2 -saturated BMP-TFSI.

On the left hand side (Figures 3a–3c), we show current traces recorded during cycling, in which the lower potential limit was shifted to more negative values by 0.2 V after the first two cycles. To determine the onset of the ORR and to distinguish it from Zn deposition, we use the ion current of $m/z = 32$ (lower panel). The onset of the faradaic current in Figure 3 is shifted to more positive potentials as compared to the ORR in neat BMP-TFSI (Figure 2). As indicated by the simultaneous onset of O_2 consumption (Figure 3b), the faradaic current results from the ORR. A similar shift of the ORR onset potential was already observed previously upon the addition of Mg^{2+} addition on a GC electrode.^{25,32,33} The lower currents in the second cycle of each potential window indicate that there is some electrode passivation. During the ORR, two electrons per O_2 molecule are transferred, which points to the formation of O_2^{2-} and, in the presence of Zn^{2+} , to the formation of deposited ZnO_2 . This resembles our previous DEMS results in 0.1 M $Mg(TFSI)_2$ containing BMP-TFSI, where we detected the formation of MgO_2 , which passivates the surface.²⁵ DEMS measurements on other divalent cations (Mg^{2+} , Ca^{2+} , Sr^{2+} , Ba^{2+}) in DMSO based perchlorate electrolytes have shown that these also favor a two-electrons transfer per O_2 molecule on Au electrodes. In contrast, on GC electrodes this is only the case for Mg^{2+} and Ba^{2+} , while Ca^{2+} and Sr^{2+} were found to favor the transfer of 1 to 1.5 electrons.²⁷

In the anodic scan, there is no peak in the faradaic current, in contrast to the observations in neat BMP-TFSI. This is in line with the results of Azaceta et al. and Tulodziecki et al., who reported that the ORR is irreversible in Zn^{2+} containing BMP-TFSI³⁰ and EMIM-TFSI.³¹ Obviously, the re-oxidation of ZnO_2 is unlikely. Again, this resembles our findings in Mg^{2+} containing BMP-TFSI, where the formation of MgO_2 is irreversible, with no features in the anodic current.²⁵ Cycling in the wider potential window (indicated by the blue curves), the passivation observed in the 2nd cycle persists, but higher ORR currents are visible when going to the more negative potentials. This goes along with a higher O_2 consumption (Figure 3b). Also in this case the ORR is irreversible and the 2nd cycle to low potentials shows again lower currents due to passivation.

On the right hand side of Figures 3d–3f, the lower potential limit is even lower and first set to -1.4 V. Starting with a freshly polished electrode, we again find an initial current increase in the first cathodic scan at potentials below 0.6 V, i.e., in the range where we later see O_2 evolution in the anodic scan, which is accompanied by O_2 consumption. At more negative potentials this is followed by two plateaus in the first cathodic scan, which also go along with O_2 consumption. This resembles our observations in neat BMP-TFSI. In the following cycles the faradaic current is slightly lower than in the first cycle, similar to the measurements in the small potential window. This indicates that the first cycle leads to some surface passivation (most likely due to the deposition of the ORR products). The number of electrons transferred per O_2 molecule starts at a value of two between 0 and -0.5 V, in agreement with the results obtained in the narrow potential window, and reaches a value of about three transferred electrons at lower potentials (see the inset of Figure 3d for the 4th cycle). Since there is no stable oxidic species resulting from a 3 electron transfer, we expect ZnO formation in parallel to peroxide formation at lower potentials. The formation of ZnO is in agreement with previous studies, where the films deposited on different electrode materials such as fluorine doped tin oxide,^{29,30} Pt, stainless steel and indium tin oxide³¹ upon reduction in $ZnTFSI_2$ containing BMP-TFSI were found to mainly consist of ZnO . This is different from the addition of Mg^{2+} (0.1 M), where MgO_2 was found as the main product of the ORR.³³ However, also side processes which do not consume O_2 , such as the Zn deposition (which at least in the absence of O_2 occurs at these potentials) or electrolyte decomposition could contribute to the higher number of transferred electrons. We can rule out, however, H_2 formation, which could be expected from reduction of water traces. In an attempt to characterize the deposits formed after extensive cycling, XRD measurements were performed after rinsing the electrode surface with acetone. However, the thickness of the resulting layer seems to be insufficient for this analysis and no characteristic signals were found (see supporting information).

In the anodic scan we observe a peak appearing already in the first cycle after scanning to low potentials, which increases during cycling until it reaches a steady state in the 4th cycle. This peak was not observed when cycling in the narrow potential window (Figures 3a–3c). In this anodic peak, O_2 formation is detected. Assuming this as the only process, this would correspond to 1.1 ± 0.05 electrons transferred per O_2 molecule (based on the integrated charges of the faradaic current over the entire peak and of the $m/z = 32$ ion current), similar to observations in Mg^{2+} containing BMP-TFSI,²⁵ which hints to the re-oxidation of superoxide. The finding that a potential excursion to very negative values during the ORR is needed before the OER can be observed in the succeeding anodic scan, closely resembles our previous findings in Mg^{2+} containing BMP-TFSI.²⁵ Interestingly, after cycling in this wide potential range, and subsequently raising the lower potential limit in the cathodic scan (blue line, Figures 3d, 3e), the anodic OER peak is still visible and the number of electrons is still one, again similar to corresponding experiments with Mg^{2+} .

In summary, the ZnO_2 formation during the ORR in the presence of Zn^{2+} appears to be irreversible with no observed OER in the anodic scan, when scanning to potentials around 0.3 V. In contrast, when cycling to lower potentials (here -1.4 V), the formation of O_2^- is enabled and an OER peak appears.

Influence of H_2O on the ORR/OER in Zn^{2+} containing IL.— Finally we also investigated the influence of water on the ORR/OER in 0.01 M $Zn(TFSI)_2$ containing BMP-TFSI. In Figure 4 we show CVs recorded in the narrow potential windows in the left column. Cycling with a cathodic limit of 0 V (red graph), we find a reductive current at $E < 0.5$ V, accompanied by O_2 consumption, as detected by DEMS. Hence, the ORR starts at 0.5 V, which is similar to the behavior in “dry” Zn^{2+} containing IL.

In this case we did not observe passivation effects in the second and third cycle, in contrast to the ORR in “dry” Zn^{2+} containing electrolyte. Possibly, water hinders either the formation or the adsorption of ZnO_2 , which was held responsible for the passivation in “dry” electrolyte. Since more than two electrons per O_2 molecule (based on the integrated charges of the faradaic current and of the $m/z = 32$ ion current) are transferred during the ORR, peroxide formation cannot be the only process in that reaction. Instead, ZnO formation or even Zn deposition seem to occur in parallel. Whatever product is formed in the narrow potential range during reduction, its formation appears to be irreversible, as no anodic current is found in the subsequent positive-going scan. Only after cycling to lower potentials (blue), we find a current peak in the anodic scan. However, there is no corresponding peak in the mass spectrometric measurements, neither in the O_2 nor in the H_2 signal. This is also true when scanning to even slightly more negative potentials, where the anodic faradaic current peak is more pronounced. Obviously, the peak in the faradaic current at 0.3 V can only stem from processes which do not evolve O_2 formation, such as Zn dissolution.

Figures 4d–4f shows a CV recorded in an expanded potential window, with a lower limit of -1.2 V, using a freshly polished electrode. Since the first and the following cycles do not differ, which is in contrast to our finding for the ORR in “dry” Zn^{2+} containing BMP-TFSI, we show only the first cycle. Going to cathodic potentials, there is only a single plateau in the cathodic current, which is also in contrast to the “dry” electrolyte. At even lower potentials, we detect H_2 evolution. In the potential range of the plateau two electrons are transferred per O_2 molecule, again pointing toward peroxide formation. H_2 evolution, indicative of electrolyte decomposition (including possible water trace impurities), starts at -1 V, i.e., at 1 V lower potential compared to O_2 -free electrolyte (see the first section). Obviously, the HER from water splitting is hindered in the presence of O_2 .

Going to anodic potentials, a current peak appears at around 0.3 V, which is paralleled also the O_2 signal. Also after narrowing the potential window, in order to cycle in a potential range where no electrolyte decomposition takes place (blue), the OER is still visible. It is again connected with a two-electron transfer per O_2 molecule, as expected for a re-oxidation of peroxide. This is different to the

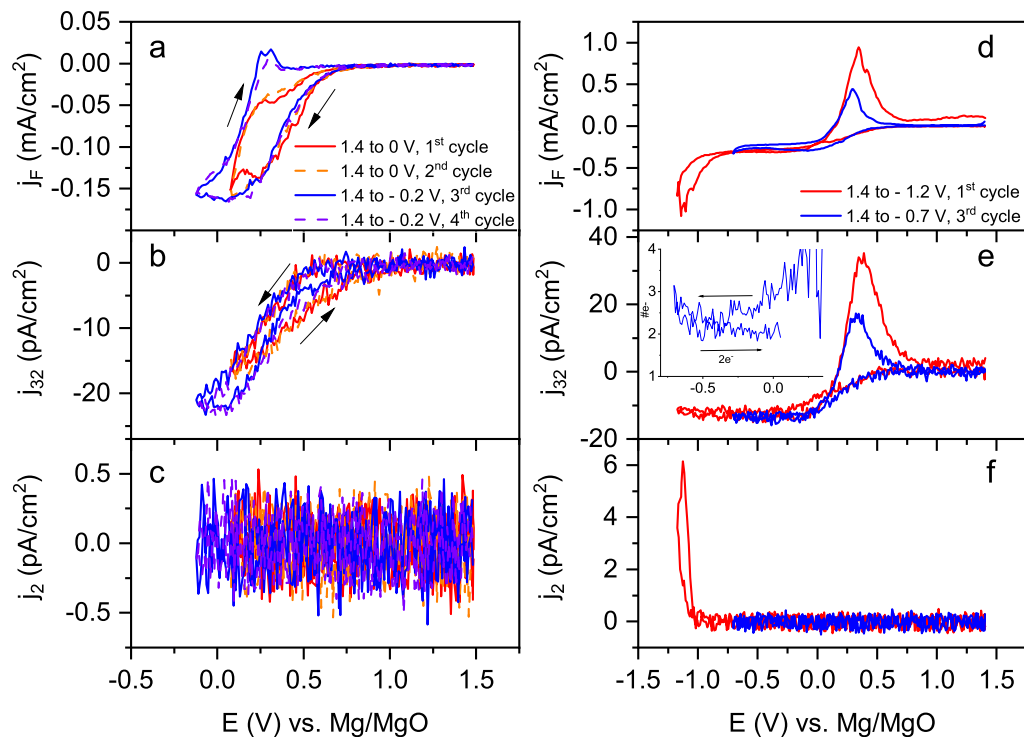


Figure 4. CVs of O₂ saturated 0.01 M Zn(TFSI)₂ with 1.1 wt% H₂O in BMP-TFSI (10 mV s⁻¹ 0.16 mL min⁻¹) on a GC electrode (top) and the corresponding ion currents of O₂ (*m/z* = 32) and H₂ (*m/z* = 2) with increasing (left) and decreasing (right) potential window. Inset: number of transferred electrons during the 3rd cycle.

measurements in Zn-free electrolyte, where only one electron per O₂ molecule is transferred during the OER, as discussed in the second section.

Additionally, after the cycling experiments (start/end of the cycle at 1.4 V vs. Mg/MgO), we again performed XRD measurements in order to identify irreversibly deposited products on the GC electrode. In contrast to the “dry” electrolytes, the results shown and discussed in the supporting information indicate mainly the formation of zinc-oxide species. Additional formation of ZnO₂ cannot be excluded, however. Nevertheless, assuming that the formation of ZnO₂ is reversible, only a small amount of this is expected to remain on the electrode surface as the CV experiment was stopped at the upper potential limit, where ZnO₂ should largely be consumed in the OER.

Discussion

In Figure 5 we present an overview about the various reactions taking place in the different BMP-TFSI based electrolyte mixtures, which were discussed separately in the preceding sections. The red numbers above the arrows indicate the onset potentials of the different reactions in the direction of the respective arrows. The different reactions can be summarized as follows:

1. In O₂-free electrolytes, the presence of Zn²⁺ in the IL electrolyte leads to a reversible Zn deposition/dissolution. On a clean GC surface Zn deposition (−0.1 V) is shifted to lower potentials to initiate Zn nucleation,³⁵ whereas in later cycles Zn deposition can be observed already at potentials < 0.1 V, equivalent to a shift of 0.2 V to more positive potentials. Although for Zn-air batteries a substantial potential difference between Zn deposition and ORR is desired, in the IL electrolyte studied here, the onset of the ORR in Zn²⁺-free BMP-TFSI is only at ~0 V, i.e., in a similar potential range as Zn deposition. The ORR first proceeds reversibly via for-

mation of a superoxide, whereas peroxide formation is observed at more negative potentials (−0.5 V).

2. In the “dry” electrolyte containing both Zn²⁺ and O₂, metallic Zn deposition plays only a minor role, and the ORR is the dominating process. In this electrolyte, the ORR proceeds via a transfer of two (at low potentials three) electrons per O₂ molecule, which results in the deposition of ZnO₂ films. At low potentials, additional processes occur, such as ZnO formation, metallic Zn deposition and electrolyte decomposition, which lead to an overall increase of the number of electrons exchanged per O₂ molecule. Under these conditions, the OER is observed only after a preceding potential excursion to very low potentials, below −1.4 V, while at higher turnaround potentials the surface appears to be passivated with no OER in the anodic scan. The OER detected after cycling to very low potentials, delivers one electron per molecule O₂ formation. This is interpreted in a picture where after cycling superoxide species are formed in the cathodic scan (possibly due to a local depletion of Zn²⁺) which are reversibly oxidized in the anodic scan producing O₂. Similar findings have been reported also for the ORR/OER upon the addition of Mg²⁺ (0.1 M) in the same IL.²⁵
3. The addition of H₂O has a positive effect on the Zn deposition (in O₂-free electrolyte) and on the ORR and OER (independent of the Zn²⁺ addition).
 - a. In Zn²⁺ containing O₂-free electrolyte, the Zn deposition occurs at higher potentials compared to “dry” electrolyte. Both, in humidified and “dry” electrolyte, the onset of Zn deposition in the first cathodic scan requires at least 0.3 V more negative potentials than the ongoing Zn deposition in the subsequent anodic scan. Thus the nucleation of Zn is a key issue for Zn deposition in both electrolytes. The positive potential shift in humidified electrolyte may be attributed to changes in the Zn²⁺ coordination changing from TFSI⁻ coordinated ions to aqueous Zn²⁺ species. This has been found by Raman spectroscopy in trifluoromethanesulfonate based ILs.¹⁹ Furthermore, the Zn

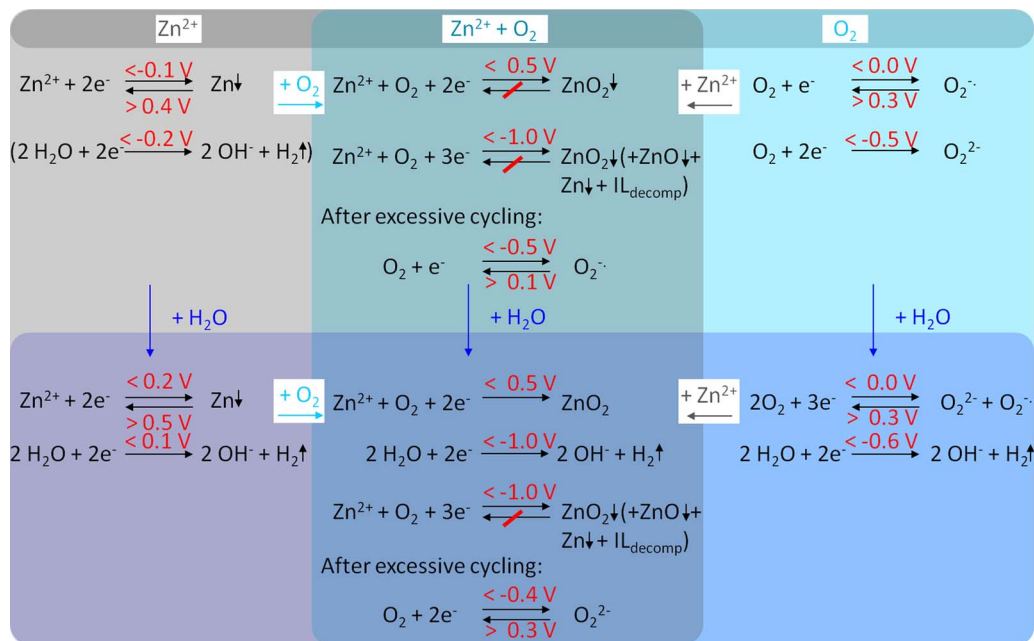


Figure 5. Schematic overview of the ongoing reactions during cycling in different electrolyte systems.

dissolution peak is sharper upon water addition, which is likely related to changes in the physicochemical properties of the electrolyte, i.e., a decreased viscosity and increased mobility of the Zn^{2+} species.^{18,36}

- The higher mobility of the electrolyte species by the addition of a protic solvent^{22,40,44} also causes an increase of the faradaic currents of ORR and OER in Zn^{2+} -free BMP-TFSI.
- Upon the addition of water to the Zn^{2+} -free electrolyte, the number of electrons transferred per O_2 molecule changes and mostly peroxides are formed. Additionally, the amount of evolved O_2 is largely enhanced after humidifying the electrolyte, which indicates that the peroxide species remain at the working electrode and are therefore oxidized again.
- In Zn^{2+} and O_2 containing electrolyte, the onset potential for ORR is at similar potentials as in “dry”, neat BMP-TFSI. After cycling to low potentials OER takes place in both humidified, O_2 containing electrolytes. The transfer of two electrons per O_2 points to the reversible formation/oxidation of H_2O_2 in the ORR/OER on the GC electrode. While no significant enhancement of the ORR/OER has been found in dry BMP-TFSI³³ when using GC or catalysts which are known to be more active in aqueous electrolytes (Pt, manganese oxides), the influence of such more active catalysts has not been studied systematically in mixed water/ILs.

Finally we would like to note that it is well known that GC is not a good catalyst for the ORR in aqueous electrolytes, since the activity is low and mostly H_2O_2 is formed instead of water.⁵³ Therefore, better catalysts such as Pt or metal oxides^{54–56} or even nanofiber materials,^{57–59} are needed and used for Zn-air batteries. In non-aqueous electrolytes, the role of the electrocatalyst on the reaction mechanism is less understood. Comparing GC, Au,³² Pt and manganese oxide catalysts,³³ no significant enhancement of the ORR/OER has been found in dry BMP-TFSI with and without the addition of Mg^{2+} . This observation may be explained by very weak interactions between the electrode surface and the superoxide anion, resulting in an outer sphere reaction mechanism.³² Similarly, Reinsberg et al. found for another non-aqueous Mg^{2+} containing electrolyte (0.4 M $Mg(ClO_4)_2$ in DMSO) that around two electrons are transferred per O_2 molecule for GC, Au and Pt electrodes, while between 3 and 4 electrons are transferred when using Rh electrodes.⁶⁰ Since the humidified BMP-TFSI

electrolytes are in between the aqueous and non-aqueous electrolytes, the influence of the electrode material would be an interesting topic for further studies.

Considering the studied mixtures as electrolytes for Zn-air batteries both, the ORR/OER and the Zn deposition/dissolution appear too sluggish for practical applications. The addition of water enhances the electrolyte properties and the reactions kinetics are improved, however, the reaction kinetics are still inferior to common aqueous electrolytes employed in Zn-air batteries. Therefore, the implicit advantages of ionic liquid electrolytes (e.g. no carbonate formation, less H_2 evolution) cannot counterbalance the drawbacks.

Conclusions

Aiming at a better understanding of the processes in secondary Zn-air batteries we have investigated the influence of water trace impurities and Zn^{2+} ions on the ORR/OER in humidified and dry BMP-TFSI on a GC electrode by online DEMS. The measurements were performed under enforced and controlled mass transport conditions. The addition of water was shown to lead to reversible peroxide formation, which is not suppressed by the addition of Zn^{2+} . This shows that the addition of water can improve the performance of air batteries with ionic liquid electrolyte. Although the presence of water improves the Zn deposition/dissolution and ORR/OER characteristics of the IL electrolyte, the kinetics of the ORR are still slow compared to aqueous electrolytes. Here the electrode material i.e., the electrocatalyst, could play a crucial role in the humidified IL electrolytes. Overall, the measurements have demonstrated the additional insights that can be gained from online spectro-electrochemical studies under well-defined reaction and transport conditions.

Acknowledgments

This work was supported by the Deutsche Forschungsgemeinschaft via project Be 1201/22-1. Zenonas Jusys acknowledges support from the German Federal Ministry of Education and Research (BMBF) in the project 03 × 4636C (“Li-EcoSafe – Entwicklung kostengünstiger und sicherer Lithium-Ionen-Batterien”). The authors would also like to thank Kaidi Zhang for his assistance with the DEMS measurements and Xin Chen of the Institute of Functional Nanosystems, Ulm University, for performing the XRD measurements. This work contributes

to the research performed at CELEST (Center for Electrochemical Energy Storage Ulm-Karlsruhe).

ORCID

J. Schnaidt  <https://orcid.org/0000-0001-6034-1534>

Z. Jusys  <https://orcid.org/0000-0003-3970-5799>

R. J. Behm  <https://orcid.org/0000-0002-7565-0628>

References

1. A. R. Mainar, E. Iruin, L. C. Colmenares, A. Kvasha, I. de Meatza, M. Bengoechea, O. Leonet, I. Boyano, Z. Zhang, and J. A. Blazquez, *J. Energy Storage*, **15**, 304 (2018).
2. Y. Li and H. Dai, *Chem. Soc. Rev.*, **43**, 5257 (2014).
3. J. S. Lee, S. Tai Kim, R. Cao, N. S. Choi, M. Liu, K. T. Lee, and J. Cho, *Adv. Energy Mater.*, **1**, 34 (2011).
4. R. Mainar, O. Leonet, M. Bengoechea, I. Boyano, I. de Meatza, A. Kvasha, A. Guerfi, and J. Alberto Blazquez, *Int. J. Energy Res.*, **40**, 1032 (2016).
5. G. Koscher and K. Kordesch, *J. Power Sources*, **136**, 215 (2004).
6. Z. L. Wang, D. Xu, J. J. Xu, and X. B. Zhang, *Chem. Soc. Rev.*, **43**, 7746 (2014).
7. M. Xu, D. G. Ivey, Z. Xie, and W. Qu, *J. Power Sources*, **283**, 358 (2015).
8. J. Fu, Z. P. Cano, M. G. Park, A. Yu, M. Fowler, and Z. Chen, *Adv. Mater.*, **29**, 1604685 (2017).
9. P. Gu, M. Zheng, Q. Zhao, X. Xiao, H. Xue, and H. Pang, *J. Mater. Chem. A*, **5**, 7651 (2017).
10. J. Fu, R. Liang, G. Liu, A. Yu, Z. Bai, L. Yang, and Z. Chen, *Adv. Mater.*, **31**, 1805230 (2019).
11. L. Jörissen, *J. Power Sources*, **155**, 23 (2006).
12. S. Liu, W. Han, B. Cui, X. Liu, F. Zhao, J. Stuart, and S. Licht, *J. Power Sources*, **342**, 435 (2017).
13. J. F. Drillet, F. Holzer, T. Kallis, S. Müller, and V. M. Schmidt, *Phys. Chem. Chem. Phys.*, **3**, 368 (2001).
14. M. Kar, T. J. Simons, M. Forsyth, and D. R. MacFarlane, *Phys. Chem. Chem. Phys.*, **16**, 18658 (2014).
15. B. Dilasari, Y. Jung, and K. Kwon, *J. Ind. Eng. Chem.*, **45**, 375 (2017).
16. T. J. Simons, D. R. MacFarlane, M. Forsyth, and P. C. Howlett, *ChemElectroChem*, **1**, 1688 (2014).
17. M. Xu, D. G. Ivey, Z. Xie, W. Qu, and E. Dy, *Electrochim. Acta*, **97**, 289 (2013).
18. T. J. Simons, A. A. J. Torriero, P. C. Howlett, D. R. MacFarlane, and M. Forsyth, *Electrochem. Commun.*, **18**, 119 (2012).
19. Z. Liu, S. Z. El Abedin, and F. Endres, *Phys. Chem. Chem. Phys.*, **17**, 15945 (2015).
20. M. S. Ghazvini, G. Pulletikurthi, T. Cui, C. Kuhl, and F. Endres, *J. Electrochem. Soc.*, **165**, D354 (2018).
21. I. M. AlNashef, M. L. Leonard, M. C. Kittle, M. A. Matthews, and J. Weidner, *Electrochem. Solid-State Lett.*, **4**, D16 (2001).
22. Y. Katayama, H. Onodera, M. Yamagata, and T. Miura, *J. Electrochem. Soc.*, **151**, A59 (2004).
23. L. Xiong, E. O. Barnes, and R. G. Compton, *Sens. Actuators, B*, **200**, 157 (2014).
24. M. Islam, B. N. Ferdousi, T. Okajima, and T. Ohsaka, *Electrochem. Commun.*, **7**, 789 (2005).
25. J. Schnaidt, T. L. Nguyen, Z. Jusys, and R. J. Behm, *Electrochim. Acta*, **299**, 372 (2019).
26. C. J. Allen, J. Hwang, R. Kautz, S. Mukerjee, E. J. Plichta, M. A. Hendrickson, and K. M. Abraham, *J. Phys. Chem. C*, **116**, 20755 (2012).
27. P. Reinsberg, A. Abd-El-Latif, and H. Baltruschat, *Electrochim. Acta*, **273**, 424 (2018).
28. C. Pozo-Gonzalo, P. C. Howlett, D. R. MacFarlane, and M. Forsyth, *Electrochem. Commun.*, **74**, 14 (2017).
29. E. Azaceta, R. Tena-Zaera, R. Marcilla, S. Fantini, J. Echeberria, J. A. Pomposo, H. Grande, and D. Mecerreyes, *Electrochem. Commun.*, **11**, 2184 (2009).
30. E. Azaceta, R. Marcilla, D. Mecerreyes, M. Ungureanu, A. Dev, T. Voss, S. Fantini, H. J. Grande, G. Cabanero, and R. Tena-Zaera, *Phys. Chem. Chem. Phys.*, **13**, 13433 (2011).
31. M. Tulodziecki, J. M. Tarascon, P. L. Taberna, and C. Guery, *J. Electrochem. Soc.*, **159**, D691 (2012).
32. Y. T. Law, J. Schnaidt, S. Brimaud, and R. J. Behm, *J. Power Sources*, **333**, 173 (2016).
33. M. Bozorgchenani, P. Fischer, J. Schnaidt, T. Diemant, R. M. Schwarz, M. Marinaro, M. Wachtler, L. Jörissen, and R. J. Behm, *ChemElectroChem*, **5**, 2600 (2018).
34. Y. S. Wang, H. W. Yeh, Y. H. Tang, C. L. Kao, and P. Y. Chen, *J. Electrochem. Soc.*, **164**, D39 (2017).
35. M. Xu, D. G. Ivey, Z. Xie, and W. Qu, *Electrochim. Acta*, **89**, 756 (2013).
36. M. Kar, B. Winther-Jensen, M. Armand, T. J. Simons, O. Winther-Jensen, M. Forsyth, and D. R. MacFarlane, *Electrochim. Acta*, **188**, 461 (2016).
37. F. R. McLarnon and E. J. Cairns, *J. Electrochem. Soc.*, **138**, 645 (1991).
38. K. Kim, Y. H. Cho, S. W. Eom, H. S. Kim, and J. H. Yeum, *Mater. Res. Bull.*, **45**, 262 (2010).
39. R. E. F. Einerhand, W. H. M. Visscher, and E. Barendrecht, *J. Appl. Electrochem.*, **18**, 799 (1988).
40. X. Z. Yuan, V. Alzate, Z. Xie, D. G. Ivey, E. Dy, and W. Qu, *J. Electrochem. Soc.*, **161**, A458 (2014).
41. A. M. O'Mahony, D. S. Silvester, L. Aldous, C. Hardacre, and R. G. Compton, *J. Chem. Eng. Data*, **53**, 2884 (2008).
42. S. Randström, M. Montanino, G. B. Appetecchi, C. Lagergren, A. Moreno, and S. Passerini, *Electrochim. Acta*, **53**, 6397 (2008).
43. E. E. Switzer, R. Zeller, Q. Chen, K. Sieradzki, D. A. Buttry, and C. Friesen, *J. Phys. Chem. C*, **117**, 8683 (2013).
44. X. Z. Yuan, V. Alzate, Z. Xie, D. G. Ivey, and W. Qu, *J. Electrochem. Soc.*, **161**, A451 (2014).
45. J. Herranz, A. Garsuch, and H. A. Gasteiger, *J. Phys. Chem. C*, **116**, 19084 (2012).
46. S. Monaco, A. M. Arangio, F. Soavi, M. Mastragostino, E. Paillard, and S. Passerini, *Electrochim. Acta*, **83**, 94 (2012).
47. A. W. Lodge, M. J. Lacey, M. Fitt, N. Garcia-Araez, and J. R. Owen, *Electrochim. Acta*, **140**, 168 (2014).
48. X. Z. Yuan, V. Alzate, Z. Xie, D. G. Ivey, E. Dy, and W. Qu, *J. Electrochem. Soc.*, **161**, A458 (2014).
49. We would like to note that we were not able to reconcile these numbers. First, the equation given by the authors is incorrect in so far as it refers to a 2- or 4-electron process at the disk reaction, which is correct in aqueous electrolytes where H₂O₂ formation needs to be discriminated from H₂O, but not for the present case. Furthermore, the ring potential applied is well in the ORR region, 2019).
50. D. Alwast, J. Schnaidt, Y. T. Law, and R. J. Behm, *Electrochim. Acta*, **197**, 290 (2016).
51. A. Khan, C. A. Gunawan, and C. Zhao, *ACS Sustainable Chem. Eng.*, **5**, 3698 (2017).
52. C. Pozo-Gonzalo, A. A. J. Torriero, M. Forsyth, D. R. MacFarlane, and P. C. Howlett, *J. Phys. Chem. Lett.*, **4**, 1834 (2013).
53. R. L. McCreery, *Chem. Rev.*, **108**, 2646 (2008).
54. M. Eckardt, K. Sakaushi, A. Lyalin, M. Wassner, N. Hüsing, T. Taketsugu, and R. J. Behm, *Electrochim. Acta*, **299**, 736 (2019).
55. M. Wassner, M. Eckardt, C. Gebauer, G. R. Bourret, N. Hüsing, and R. J. Behm, *Electrochim. Acta*, **227**, 367 (2017).
56. M. H. Seo, S. M. Choi, H. J. Kim, and W. B. Kim, *Electrochem. Commun.*, **13**, 182 (2011).
57. J. Bian, Z. Li, N. Li, and C. Sun, *Inorg. Chem.*, **58**, 8208 (2019).
58. J. Bian, R. Su, Y. Yao, J. Wang, J. Zhou, F. Li, Z. L. Wang, and C. Sun, *ACS Appl. Energy Mater.*, **2**, 923 (2019).
59. X. Zhang, Y. Gong, S. Li, and C. Sun, *ACS Catal.*, **7**, 7737 (2017).
60. P. Reinsberg, C. Bondue, and H. Baltruschat, *Electrochim. Acta*, **200**, 214 (2016).